

Development of Carbon Supported Perovskite-Oxide for Lithium Ions Battery Application

Lijie He^{1,*}, Dong Zhang², Peng Du¹, Gianglei Tan¹, Tao Mu¹ and Haiyan Liu¹

¹ YingKou Institute of Technology, No.46 Bowen Rd, YingKou, LiaoNing, 115014, P.R.China

² Key Laboratory of Physics and Technology for Advanced Batteries (Ministry of Education), College of Physics, JinLin University, Changchun, Jilin, 130021, P.R.China

*E-mail: helijie80@163.com

Received: 1 March 2017 / Accepted: 29 March 2017 / Published: 12 May 2017

Perovskite-type oxide catalyst-based carbon electrodes were studied as air electrodes for aqueous lithium-air secondary batteries, which were comprised of a carbon black air electrode with $\text{La}_{0.8}\text{Sr}_{0.2}\text{Fe}_{0.8}\text{Mn}_{0.2}\text{O}_3$ catalyst, an aqueous electrolyte solution of saturated LiOH with 10 M LiCl, and a water-stable lithium electrode. The oxygen evolution reaction (OER) and oxygen reduction reaction (ORR) benefited from the expanded surface area of $\text{La}_{0.8}\text{Sr}_{0.2}\text{Fe}_{0.8}\text{Mn}_{0.2}\text{O}_3$ during charge and discharge. The $\text{La}_{0.8}\text{Sr}_{0.2}\text{Fe}_{0.8}\text{Mn}_{0.2}\text{O}_3$ electrocatalyst-based lithium-air batteries showed desirable cycle stability and rate capability, low overpotential, increased specific capacity of initial discharge and other improved electrochemical behaviors.

Keywords: $\text{La}_{0.8}\text{Sr}_{0.2}\text{Fe}_{0.8}\text{Mn}_{0.2}\text{O}_3$; Perovskite; Lithium-air secondary batteries; Catalyst; Oxygen reduction reaction; Oxygen evolution reaction

1. INTRODUCTION

In 1996, Abraham and Jiang reported a nonaqueous electrolyte-based lithium-oxygen battery system. Then, in 2006, Bruce and co-workers investigated the rechargeability of this system [1-13]. The theoretical energy density of rechargeable lithium-oxygen (or lithium-air) batteries, which is near that of gasoline, is superbly significant, namely, 5200 Wh/kg (including oxygen), which is 5–10 times higher than that of the latest Li-ion batteries (LIBs). Thus, conventional LIBs are likely to be replaced by rechargeable lithium-air batteries in renewable energy storage, electric vehicles (EVs) and other fields that have worldwide appeal [14-17]. Nevertheless, their particularly short cycle life, electrolyte instability, low round-trip efficiency due to the extremely undesirable overpotentials in ORR and OER, unfavorable rate capability and other drawbacks must be solved before lithium-air batteries can be

applied to real situations [18-20]. Herein, to improve the electrochemical behavior of rechargeable nonaqueous lithium-air batteries, a wide range of investigations are thus performed to address these disadvantages. The essential aspect is the air electrode, in particular the effectiveness of the electrocatalyst in OER and ORR.

The exploration of highly efficient bifunctional catalysts for ORR and OER and the fabrication of novel structures for air electrodes constitute two major techniques for the optimization of air electrodes [16, 21-27]. Heterogeneous composite catalysts, carbon materials, transition metal oxide catalysts, noble catalysts based on palladium (Pd)/platinum (Pt) and other materials have been researched following the former technique. The behavior of lithium-air batteries can be enhanced by decreasing the overpotential and effective acceleration of OER and ORR using a perfect bifunctional catalyst. A significant improvement in the rate capacity and kinetics of OER and ORR can be achieved by expanding the specific surface area (containing adequate effective active sites), and thus, it is essential for novel air electrodes to be designed in terms of the latter strategy. At the same time, an improvement in cycling behavior and discharge capacity and the accommodation of insoluble discharge products can be enhanced by ample void volumes and open frameworks present in the architecture. Vertically aligned carbon nanotubes, hierarchically porous functionalized graphene sheets, traditional porous composites and other diverse electrode frameworks have been investigated; however, a uniform standard has not been obtained yet.

Perovskite oxides, which have desirable oxygen mobility, comparatively significant conductivity for ions and electrons and a defect framework, are appealing electrocatalysts, compared to their counterparts [28-30]. Yang et al. prepared a Cu nanoparticle-loaded $\text{Sr}_{0.95}\text{Ce}_{0.05}\text{CoO}_3$ perovskite oxide and applied it in Li-air batteries with organic/aqueous doped electrolyte as a bifunctional catalyst [29]. Zhao et al. prepared hierarchical mesoporous perovskite $\text{La}_{0.5}\text{Sr}_{0.5}\text{CoO}_{2.91}$ nanowires and employed them in lithium-air batteries as a bifunctional catalyst, achieving an ultrahigh capacity of 11,000 mAh/g [29]. Herein, we characterized the catalytic activity of $\text{La}_{0.8}\text{Sr}_{0.2}\text{Fe}_{0.8}\text{Mn}_{0.2}\text{O}_3$ for ORR and OER and applied the material in lithium-air batteries. The lithium-air batteries using $\text{La}_{0.8}\text{Sr}_{0.2}\text{Fe}_{0.8}\text{Mn}_{0.2}\text{O}_3$ show an enhanced specific capacity, rate capability, and cycle stability.

2. EXPERIMENTS

All reagents were of analytical grade and used without further purification. Citric acid precursors were employed for the synthesis of $\text{La}_{0.8}\text{Sr}_{0.2}\text{Fe}_{0.8}\text{Mn}_{0.2}\text{O}_3$ (LSFM), which were dissolved with the corresponding metal nitrates into 1 M aqueous citric acid solution. The as-prepared solution was dried at 60 °C until it was viscous. Then, the as-prepared syrup-like solution was heated at 60 °C for 5 h, followed by calcination at 700 °C in air for 2 h.

An air diffusion layer and a reaction layer were included in the air electrodes, where the former layer was produced through the attachment of carbon paper (0.30 mm) onto the electrode, while a binder of polytetrafluoroethylene (PTFE), the $\text{La}_{0.8}\text{Sr}_{0.2}\text{Fe}_{0.8}\text{Mn}_{0.2}\text{O}_3$ catalyst and a Ketjen black EC-600JD carbon substrate were combined to produce the latter layer. LiOH–LiCl electrolyte with a pH of 9 (roughly) provided the platform for testing the electrode. The reference electrode and counter

electrode were Hg/HgO and a platinum plate with a platinum black, respectively, and the working electrode had an active area of 0.64 cm^2 . The three electrodes comprised the test cell. An air pump was employed for adequate air supply, and the experiments were conducted at ambient temperature. The ratio of PTFE-KB for the KB electrode in the absence of catalyst was 15:85, and the ratio of PTFE-catalyst-KB by weight was 15:30:55. To affix PTFE on the Ti mesh, the electrode mixture was dried at $80 \text{ }^\circ\text{C}$ for 12 h, followed by heating at $350 \text{ }^\circ\text{C}$.

Cu $K\alpha$ radiation was adopted for X-ray diffraction analysis to obtain the confirmation of the perovskite phase. A gas adsorption analyzer was utilized to measure the Brunauer–Emmett–Teller (BET) surface area. A multi-channel potentiostat/galvanostat (Bio Logic, VMP3) at a scan rate of 10 mV/s was applied to measure the cyclic voltammetry (CV) profiles, and a potentiostat/galvanostat was used to measure the polarization profiles. An electrochemical interface and an impedance/gain phase analyzer over a frequency range of 1 MHz to 0.01 Hz was employed for AC impedance spectroscopy. All electrochemical measurements were carried out at room temperature.

3. RESULTS AND DISCUSSION

A perovskite-type oxide with a single phase and no impurity phases was revealed in the XRD profiles of the prepared $\text{La}_{0.8}\text{Sr}_{0.2}\text{Fe}_{0.8}\text{Mn}_{0.2}\text{O}_3$ powders. $\text{La}_{0.8}\text{Sr}_{0.2}\text{Fe}_{0.8}\text{Mn}_{0.2}\text{O}_3$ at ambient temperature before and after immersion into the LiOH–LiCl electrolyte was characterized via XRD, as shown in Figure 1. As shown in Figure 1, the precursor primarily generated the expected $\text{La}_{0.8}\text{Sr}_{0.2}\text{Fe}_{0.8}\text{Mn}_{0.2}\text{O}_3$ phase (PDF code 01-089-5719) [31]. No obvious variation in the XRD pattern was observed after immersion. Herein, the stability of this perovskite-type oxide in the electrolyte adopted in the aqueous lithium-air battery is examined through XRD analysis.

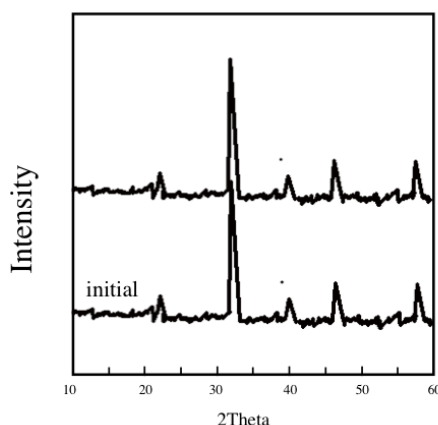


Figure 1. XRD patterns of $\text{La}_{0.8}\text{Sr}_{0.2}\text{Fe}_{0.8}\text{Mn}_{0.2}\text{O}_3$ before and after immersion in a saturated LiOH aqueous solution with 10 M LiCl.

The pore size distribution of the as-prepared $\text{La}_{0.8}\text{Sr}_{0.2}\text{Fe}_{0.8}\text{Mn}_{0.2}\text{O}_3$ is shown in Figure 2A, as well as the nitrogen adsorption-desorption isotherm, while Figure 2B shows the pore size distribution

and CO₂ adsorption-desorption isotherm. In the inset of Figure 2A, the pore size distribution revealed the absence of mesopores, and the presence of a similar type I isotherm was also observed. To measure the size of the micropores, as indicated by the N₂ adsorption-desorption isotherm, CO₂ was used as the adsorbate rather than N₂, as CO₂ provides better quantitative evaluation within the micropore range. The CO₂ isotherm was of type I, which revealed the microporous properties of the as-prepared La_{0.8}Sr_{0.2}Fe_{0.8}Mn_{0.2}O₃. An increased number of effective catalytic active sites was achieved, with a pore volume of 0.089 cm³/g, an average pore size of 1.3 nm, and a specific surface area of 21.3 m²/g, as indicated through the CO₂ adsorption-desorption isotherm. The high specific surface area and small pore size could benefit the penetration and diffusion of lithium ions.

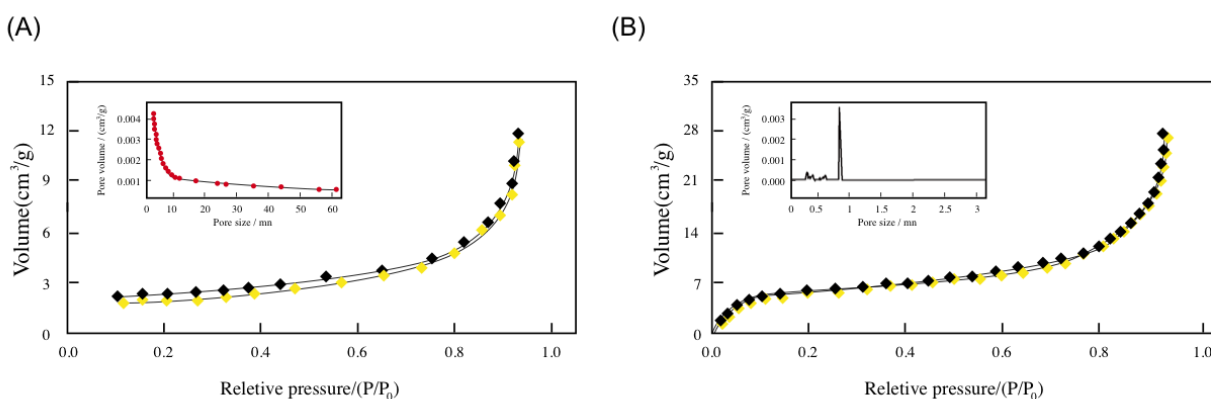


Figure 2. (A) N₂ adsorption-desorption isotherm and pore distribution plot (inset) of La_{0.8}Sr_{0.2}Fe_{0.8}Mn_{0.2}O₃; (B) CO₂ adsorption-desorption isotherm and pore distribution plot (inset) of La_{0.8}Sr_{0.2}Fe_{0.8}Mn_{0.2}O₃.

First, the electrochemical catalytic activity of La_{0.8}Sr_{0.2}Fe_{0.8}Mn_{0.2}O₃ in ORR and OER was evaluated in KOH solution (0.1 M) saturated with O₂ prior to assembling and testing the lithium-air batteries. Under identical experimental circumstances, pure and commercial Pt/C (20 wt.% Pt) carbon electrocatalysts were examined for comparison. Normalization was achieved through the geometric surface area for the obtained currents (2500 rpm). The ORR activity was in the order of pure C < La_{0.8}Sr_{0.2}Fe_{0.8}Mn_{0.2}O₃ < Pt/C (Figure 3A), and 120 mV (roughly), -6.65 mA/cm², -6.34 mA/cm² were obtained for the semi-wave potential difference in Pt/C and La_{0.8}Sr_{0.2}Fe_{0.8}Mn_{0.2}O₃, the Pt/C diffusion limiting current density and the La_{0.8}Sr_{0.2}Fe_{0.8}Mn_{0.2}O₃ diffusion limiting current density, respectively. Note that the last two values are similar. There is a desirable comparability between La_{0.8}Sr_{0.2}Fe_{0.8}Mn_{0.2}O₃ and Pt/C activity, since the Pt/C values correspond well with the Pt/C semi-wave potential and the tested diffusion limiting current density. The anodic linear sweep voltammograms for OER of these four catalysts coated on a rotating disk electrode in O₂-saturated 0.1 M KOH solution at 1600 rpm were also measured (Figure 3B). Although La_{0.8}Sr_{0.2}Fe_{0.8}Mn_{0.2}O₃ is the most active for ORR among previously reported perovskite oxides, it has low intrinsic activity for OER [32-34]. From Figure 3B, it can be clearly observed that La_{0.8}Sr_{0.2}Fe_{0.8}Mn_{0.2}O₃ demonstrated lower activity for OER than Pt/C; however, an enhanced activity was obtained compared to La_{0.8}Sr_{0.2}Fe_{0.8}Mn_{0.2}O₃ particles and pure C.

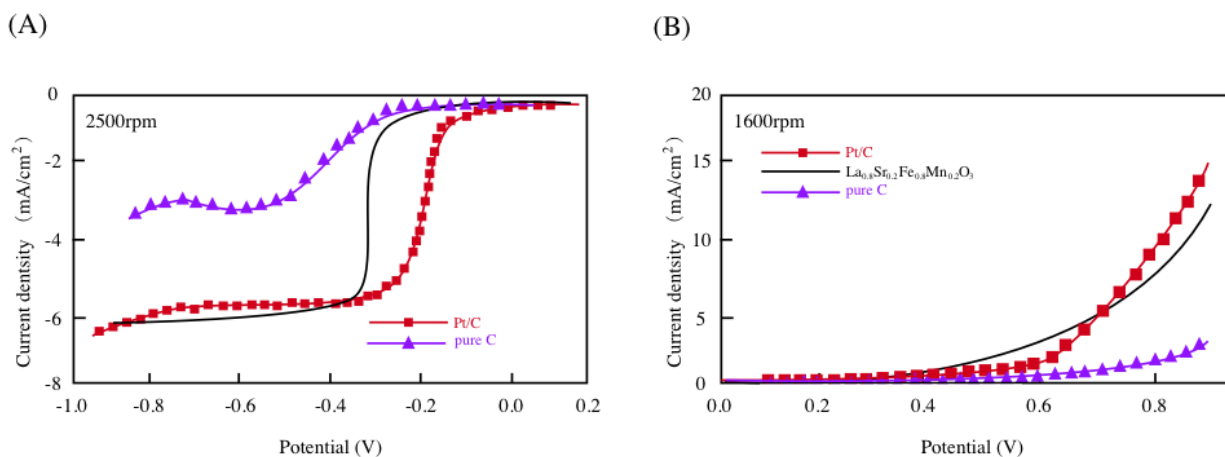


Figure 3. (A) Linear sweep voltammograms (LSVs) of the as-prepared La_{0.8}Sr_{0.2}Fe_{0.8}Mn_{0.2}O₃, pure C and commercial Pt/C in O₂-saturated 0.1 M KOH solution at 2500 rpm; (B) Comparison of their catalytic activity for OER in O₂-saturated 0.1 M KOH solution at 1600 rpm.

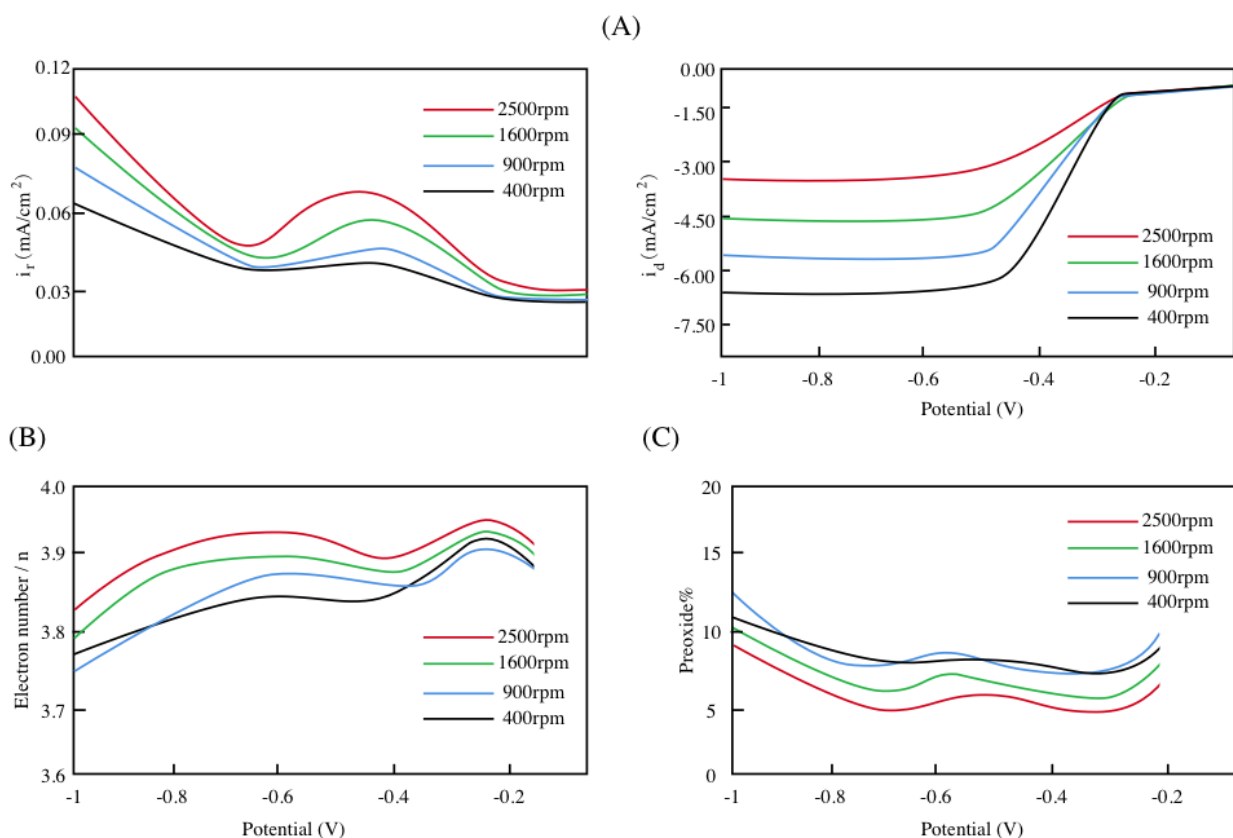


Figure 4. Disk (*i_d*) and ring (*i_r*) current densities of La_{0.8}Sr_{0.2}Fe_{0.8}Mn_{0.2}O₃ for (A) ORR, (B) electron transfer number (*n*) and (C) peroxide HO₂⁻ calculated with *i_d* and *i_r*.

To evaluate the kinetic parameters for ORR of the La_{0.8}Sr_{0.2}Fe_{0.8}Mn_{0.2}O₃ catalyst, measurements were performed over a range of rotation speeds (ω) (400-2500 rpm) in the cathodic sweep (10 mV/s). Figure 4 reveals the current density of the disk and ring (*i_d* and *i_r*). With the increase in rotation speed over 400-2500 rpm, an increase in the diffusion limiting current density was

observed. The currents increased as the speed of oxygen fluxing to the surface of the electrode increased at elevated rotation speed [35]. Figure 4B shows the transferred electron number (n), while Figure 4C indicates the contents of peroxide HO_2^- during the ORR process via i_r and i_d profiles. A $4e^-$ pathway for $\text{La}_{0.8}\text{Sr}_{0.2}\text{Fe}_{0.8}\text{Mn}_{0.2}\text{O}_3$ in ORR was observed, as the obtained HO_2^- yields were lower than 16.0% and the n values were between 3.7 and 4.0 over the measured potential range.

The inner capacity of the $\text{La}_{0.8}\text{Sr}_{0.2}\text{Fe}_{0.8}\text{Mn}_{0.2}\text{O}_3$ perovskite oxide for OER is at least one order of magnitude higher than that of the modern iridium oxide catalyst under alkaline conditions. Thus, $\text{La}_{0.8}\text{Sr}_{0.2}\text{Fe}_{0.8}\text{Mn}_{0.2}\text{O}_3$ is a potential OER catalyst. Furthermore, CV was performed in O_2 -saturated 0.1 M KOH at a scan rate of 50 mV/s at 2500 rpm between -1.0 V and 1.0 V to evaluate the stability of the $\text{La}_{0.8}\text{Sr}_{0.2}\text{Fe}_{0.8}\text{Mn}_{0.2}\text{O}_3$ catalyst in ORR and OER. After 500 CV cycles, comparative stability was observed for ORR, and a mild decline was observed for OER (Figure 5), indicating the stability and reversibility of the catalytic activity for ORR and OER.

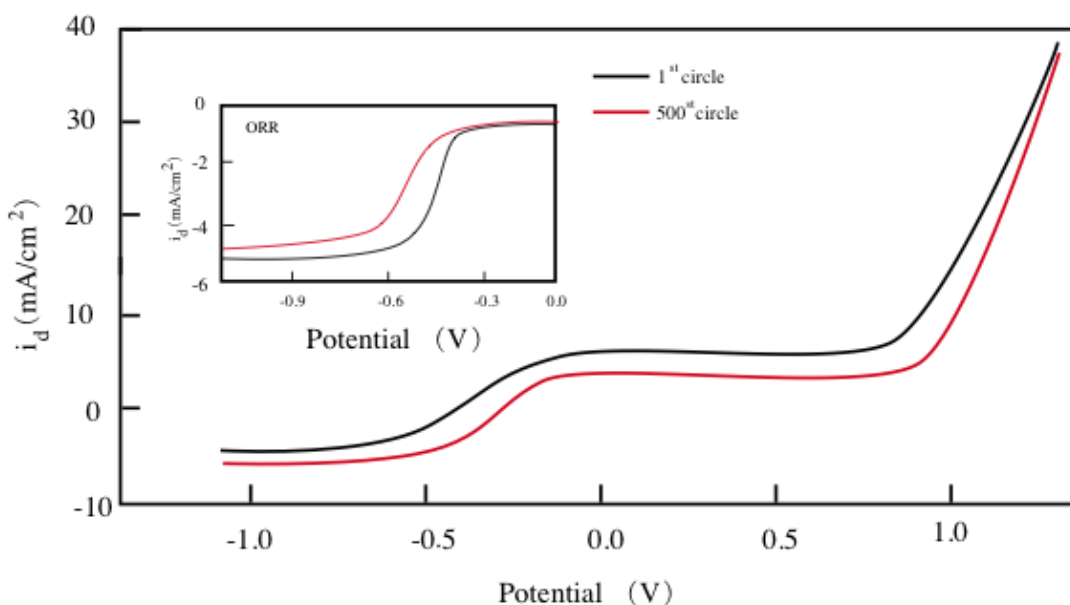


Figure 5. ORR and OER of $\text{La}_{0.8}\text{Sr}_{0.2}\text{Fe}_{0.8}\text{Mn}_{0.2}\text{O}_3$ during the 1st and 500th cycle.

A pure acetylene black electrode was examined for comparison with the electrocatalytic activity of $\text{La}_{0.8}\text{Sr}_{0.2}\text{Fe}_{0.8}\text{Mn}_{0.2}\text{O}_3$ in lithium-air batteries. Figure 6A displays the ORR and OER catalytic activity of $\text{La}_{0.8}\text{Sr}_{0.2}\text{Fe}_{0.8}\text{Mn}_{0.2}\text{O}_3$ over 4.5-2.0 V in electrolyte via CV. The $\text{La}_{0.8}\text{Sr}_{0.2}\text{Fe}_{0.8}\text{Mn}_{0.2}\text{O}_3$ -based electrode showed a higher peak current for ORR/OER than the pure acetylene black-based electrode. The ORR onset potential of 2.85 V of the former electrode is more elevated than that of the latter. The lithium-air battery round-trip efficiency, recharging features and output of energy can be enhanced as the ORR/OER kinetics are elevated.

As indicated in Figure 6B, the three different air electrode catalysts in lithium-air batteries were characterized by the initial discharge/charge patterns, in particular their discharge and charge current density (200 mA/g). Initial discharge capacities of 1820 and 6780 mAh/g were observed for the pure acetylene black-based lithium-air battery and the $\text{La}_{0.8}\text{Sr}_{0.2}\text{Fe}_{0.8}\text{Mn}_{0.2}\text{O}_3$ -based lithium-air battery,

respectively. In catalytic reactions, the chemical properties of used catalysts are essential in determining the catalytic activity [36]. The round-trip efficiency is thus enhanced through the improvement of the charge and discharge voltage in the $\text{La}_{0.8}\text{Sr}_{0.2}\text{Fe}_{0.8}\text{Mn}_{0.2}\text{O}_3$ -based lithium-air battery, where the former voltage shows more significant improvement. The pure acetylene black electrode-based lithium-air battery exhibits approximately 140 mV lower discharge voltage compared to the $\text{La}_{0.8}\text{Sr}_{0.2}\text{Fe}_{0.8}\text{Mn}_{0.2}\text{O}_3$ -based lithium-air battery. However, the pure acetylene black-based lithium-air battery exhibits a higher average charge voltage than the $\text{La}_{0.8}\text{Sr}_{0.2}\text{Fe}_{0.8}\text{Mn}_{0.2}\text{O}_3$ -based lithium-air battery.

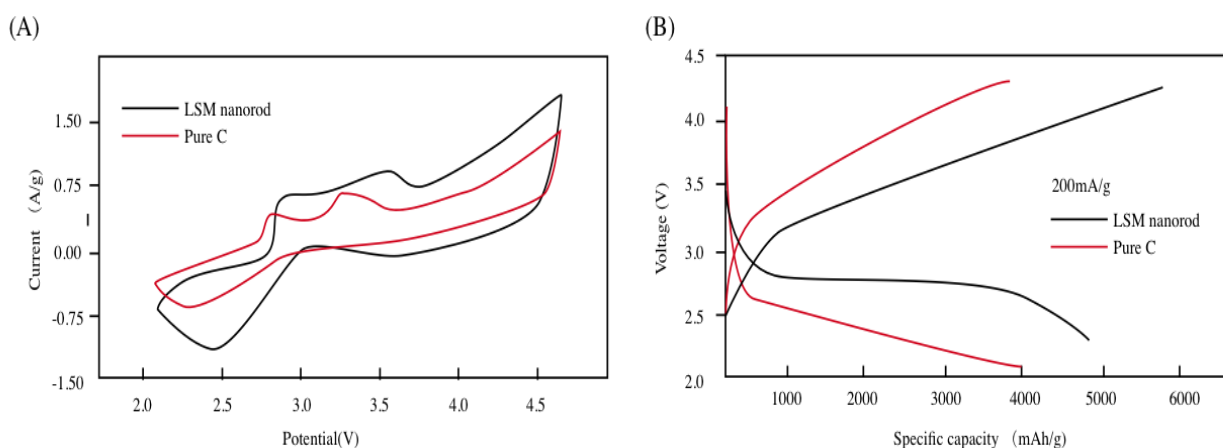


Figure 6. (A) CV curves of the $\text{La}_{0.8}\text{Sr}_{0.2}\text{Fe}_{0.8}\text{Mn}_{0.2}\text{O}_3$ -based and pure acetylene black-based lithium-air batteries at a scan rate of 0.2 mV/s; (B) Comparison of the first discharge-charge curves of the different lithium-air batteries at 200 mA/g.

The rate capacity of the $\text{La}_{0.8}\text{Sr}_{0.2}\text{Fe}_{0.8}\text{Mn}_{0.2}\text{O}_3$ -based lithium-air batteries was investigated through the discharge and charge patterns in the initial cycle at 100 mA/g, 200 mA/g and 400 mA/g (current densities) (Figure 7A). The rate capacity was found to be desirable, since there is a drop-in voltage gap between the charge and discharge plateaus and an increase in discharge capacity (4830-8750 mAh/g), corresponding to a decrease in current density (400-100 mA/g). The electrochemical performance of the $\text{La}_{0.8}\text{Sr}_{0.2}\text{Fe}_{0.8}\text{Mn}_{0.2}\text{O}_3$ electrode was compared with previous studies, as shown in Table 1. The as-prepared composite displays competitive comprehensive electrochemical properties, implying that the composite has a promising future applications. Since the electrolyte is unstable and discharge products accumulate, discharge and charge stability is especially difficult to achieve. Note that the stability is of crucial significance to nonaqueous lithium-air batteries. Previous literature has revealed that the optimal catalysts could improve the cycle performance. Figure 7B indicates that the $\text{La}_{0.8}\text{Sr}_{0.2}\text{Fe}_{0.8}\text{Mn}_{0.2}\text{O}_3$ -based lithium-air battery has a desirable cycle performance stability over 5 cycles, with a discharge and charge depth as deep as 200 mA/g. A plateau of more than 4000 mAh/g is observed for the specific capacity with a 54% retention after 5 complete discharge-charge cycles.

Table 1. Comparison of the $\text{La}_{0.8}\text{Sr}_{0.2}\text{Fe}_{0.8}\text{Mn}_{0.2}\text{O}_3$ electrode with similar electrodes reported in the literature.

Material	Specific capacity (mAh/g)	Current density (mA/g)	Reference
$\text{Co}_3\text{O}_4\text{-CoO/C}$	580	89	[37]
$\text{Co}_3\text{O}_4/\text{graphene}$	740	178	[38]
$\text{Co}_3\text{O}_4/\text{C}$	1150	222	[39]
$\text{La}_{0.8}\text{Sr}_{0.2}\text{Fe}_{0.8}\text{Mn}_{0.2}\text{O}_3$	1000	145	This work

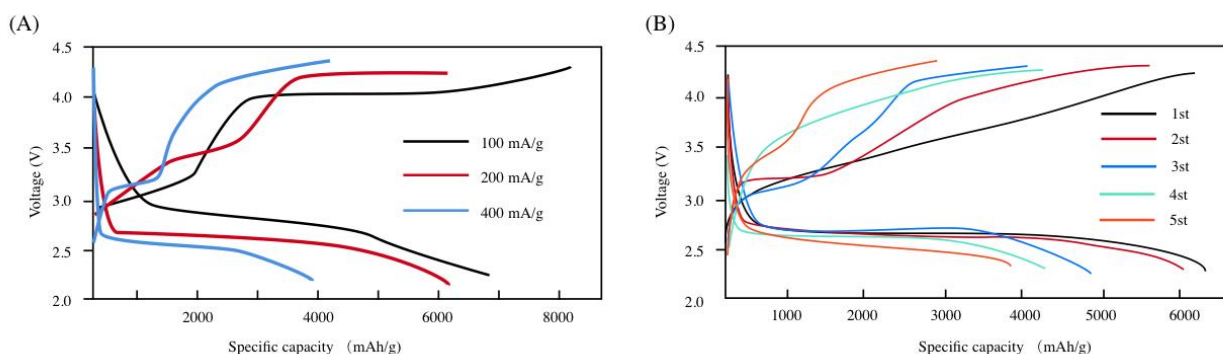


Figure 7. (A) Rate capacities of lithium-air batteries based on the $\text{La}_{0.8}\text{Sr}_{0.2}\text{Fe}_{0.8}\text{Mn}_{0.2}\text{O}_3$ catalyst under different current densities; (B) Typical discharge-charge voltage profiles.

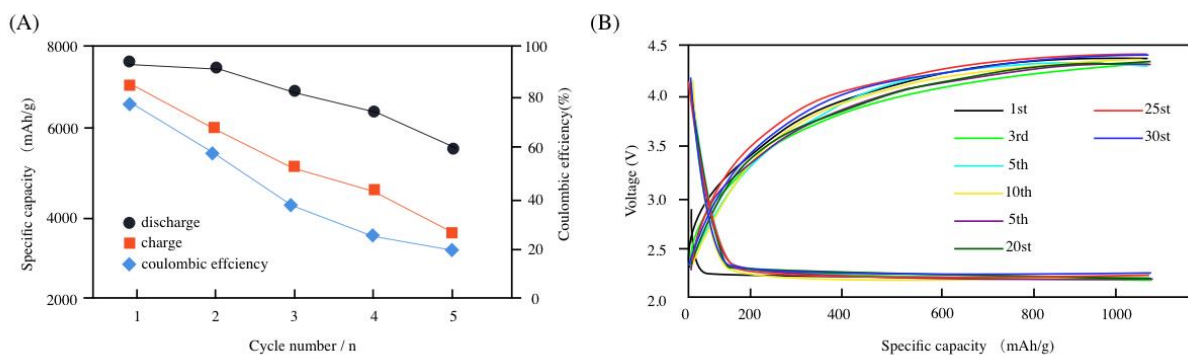


Figure 8. (A) Cycling performances during the first 5 cycles of the $\text{La}_{0.8}\text{Sr}_{0.2}\text{Fe}_{0.8}\text{Mn}_{0.2}\text{O}_3$ catalyst-based lithium-air battery at 200 mA/g between 2.0 and 4.4 V; (B) Cycling stability of the $\text{La}_{0.8}\text{Sr}_{0.2}\text{Fe}_{0.8}\text{Mn}_{0.2}\text{O}_3$ -based lithium-air battery under a specific capacity limit of 1000 mAh/g at 200 mA/g.

Figure 8A indicates that the coulombic efficiency of the $\text{La}_{0.8}\text{Sr}_{0.2}\text{Fe}_{0.8}\text{Mn}_{0.2}\text{O}_3$ -based lithium-air battery is over 75%, denoting a desirable charging efficiency. The discharging and charging capacities were similar. After 5 complete discharge-charge cycles, the battery was cycled at 200 mA/g with a specific capacity limit of 1000 mAh/g for further confirmation of the stability of the $\text{La}_{0.8}\text{Sr}_{0.2}\text{Fe}_{0.8}\text{Mn}_{0.2}\text{O}_3$ -based lithium-air battery. The $\text{La}_{0.8}\text{Sr}_{0.2}\text{Fe}_{0.8}\text{Mn}_{0.2}\text{O}_3$ catalyst was shown to

possess desirable stability, as suggested by the final discharge voltage being over 2.65 V after 30 cycles, showing only 1.4% voltage loss (Figure 8B).

4. CONCLUSIONS

The catalytic activities of a $\text{La}_{0.8}\text{Sr}_{0.2}\text{Fe}_{0.8}\text{Mn}_{0.2}\text{O}_3$ perovskite-type oxide for ORR and OER were examined in an electrolyte composed of a saturated LiOH aqueous solution with 10 M LiCl. As an electrocatalyst, $\text{La}_{0.8}\text{Sr}_{0.2}\text{Fe}_{0.8}\text{Mn}_{0.2}\text{O}_3$ is more stable and active for ORR and OER than the commercial Pt/C electrocatalyst under alkaline conditions. A significant specific capacity was achieved for the $\text{La}_{0.8}\text{Sr}_{0.2}\text{Fe}_{0.8}\text{Mn}_{0.2}\text{O}_3$ -based lithium-air battery with significant catalytic activity.

References

1. U. Paulus, U. Endruschat, G. Feldmeyer, T. Schmidt, H. Bönemann and R. Behm, *J. Catal.*, 195 (2000) 383.
2. P. Bruce, L. Hardwick and K. Abraham, *MRS Bulletin*, 36 (2011) 506.
3. C. Wang, L. Chen, Y. Su, G. Yang and W. Zhang, *Electrochimica Acta*, 213 (2016) 375.
4. M. Kunduraci, *Journal of Solid State Electrochemistry*, 20 (2016) 2105.
5. Y. Makimura, T. Sasaki, H. Oka, C. Okuda, T. Nonaka, Y. Nishimura, S. Kawauchi and Y. Takeuchi, *Journal of The Electrochemical Society*, 163 (2016) A1450.
6. A. Schilling, J. Schmitt, F. Dietrich and K. Dröder, *Energy Technology*, 4 (2016) 1502.
7. K. Wang, W. Ren, J. Yang, R. Tan, Y. Liu and F. Pan, *RSC Advances*, 6 (2016) 47723.
8. P. Zhou, H. Meng, Z. Zhang, C. Chen, Y. Lu, J. Cao, F. Cheng and J. Chen, *Journal of Materials Chemistry A*, (2017)
9. Z. Lin, A. McCreary, N. Briggs, S. Subramanian, K. Zhang, Y. Sun, X. Li, N. Borys, H. Yuan and S. Fullerton-Shirey, *2D Materials*, 3 (2016) 042001.
10. W. Zhang, Q. Wang, Y. Chen, Z. Wang and A. Wee, *2D Materials*, 3 (2016) 022001.
11. R. Woodward, R. Murray, C. Phelan, R. de Oliveira, T. Runcorn, E. Kelleher, S. Li, E. de Oliveira, G. Fechine and G. Eda, *2D Materials*, 4 (2016) 011006.
12. H. Jo, J. Lyu, R. Ruoff, H. Lim, S. Yoon, H. Jeong, T. Shin, C. Bielawski and H. Shin, *2D Materials*, 4 (2016) 014005.
13. L. Cançado, M. da Silva, E. Ferreira, F. Hof, K. Kampioti, K. Huang, A. Pénicaud, C. Achete, R. Capaz and A. Jorio, *2D Materials*, 4 (2017) 025039.
14. P. Bruce, S. Freunberger, L. Hardwick and J. Tarascon, *Nature materials*, 11 (2012) 19.
15. Z. Peng, S. Freunberger, Y. Chen and P. Bruce, *Science*, 337 (2012) 563.
16. Y. Lu and Y. Shao-Horn, *The journal of Physical Chemistry Letters*, 4 (2012) 93.
17. C. Laoire, S. Mukerjee, K. Abraham, E. Plichta and M. Hendrickson, *J Phys Chem C*, 114 (2010) 9178.
18. M. Park, H. Sun, H. Lee, J. Lee and J. Cho, *Advanced Energy Materials*, 2 (2012) 780.
19. G. Girishkumar, B. McCloskey, A. Luntz, S. Swanson and W. Wilcke, *The Journal of Physical Chemistry Letters*, 1 (2010) 2193.
20. M. Thotiyl, S. Freunberger, Z. Peng and P. Bruce, *Journal of the American Chemical Society*, 135 (2012) 494.
21. L. Fan, X. Fang, X. Wang, Y. Zeng, Y. Xiao, Z. Yu, X. Xu, Y. Hu and K. Cen, *Applied Energy*, 110 (2013) 163.
22. Y. Lu, H. Gasteiger and Y. Shao-Horn, *Journal of the American Chemical Society*, 133 (2011) 19048.

23. J. Xiao, D. Mei, X. Li, W. Xu, D. Wang, G. Graff, W.D. Bennett, Z. Nie, L. Saraf and I. Aksay, *Nano Letters*, 11 (2011) 5071.
24. J. Xu, Z. Wang, D. Xu, L. Zhang and X. Zhang, *Nature Communications*, 4 (2013)
25. X. Han, Y. Hu, J. Yang, F. Cheng and J. Chen, *Chemical Communications*, 50 (2014) 1497.
26. J. Xu, D. Xu, Z. Wang, H. Wang, L. Zhang and X. Zhang, *Angewandte Chemie International Edition*, 52 (2013) 3887.
27. X. Sun, W. Si, X. Liu, J. Deng, L. Xi, L. Liu, C. Yan and O. Schmidt, *Nano Energy*, 9 (2014) 168.
28. C. Jin, X. Cao, L. Zhang, C. Zhang and R. Yang, *Journal of Power Sources*, 241 (2013) 225.
29. Y. Zhao, L. Xu, L. Mai, C. Han, Q. An, X. Xu, X. Liu and Q. Zhang, *Proceedings of the National Academy of Sciences*, 109 (2012) 19569.
30. J. Shui, F. Du, C. Xue, Q. Li and L. Dai, *ACS Nano*, 8 (2014) 3015.
31. R. Sonntag, S. Neov, V. Kozhukharov, D. Neov and J. Ten Elshof, *Physica B: Condensed Matter*, 241 (1997) 393.
32. J. Suntivich, H. Gasteiger, N. Yabuuchi, H. Nakanishi, J. Goodenough and Y. Shao-Horn, *Nature Chemistry*, 3 (2011) 546.
33. J. Li, J. Li, H. Meng, S. Xie, B. Zhang, L. Li, H. Ma, J. Zhang and M. Yu, *Journal of Materials Chemistry A*, 2 (2014) 2934.
34. M. Risch, K. Stoerzinger, S. Maruyama, W. Hong, I. Takeuchi and Y. Shao-Horn, *Journal of the American Chemical Society*, 136 (2014) 5229.
35. S. Sankarasubramanian, J. Seo, F. Mizuno, N. Singh and J. Prakash, *Journal of The Electrochemical Society*, 163 (2016) A2377.
36. W. Zhou, Z. Shao, R. Ran, H. Gu, W. Jin and N. Xu, *Journal of the American Ceramic Society*, 91 (2008) 1155.
37. Q. Xie, Y. Ma, D. Zeng, X. Zhang, L. Wang, G. Yue and D.-L. Peng, *ACS applied materials & interfaces*, 6 (2014) 19895.
38. B. Li, H. Cao, J. Shao, G. Li, M. Qu and G. Yin, *Inorganic chemistry*, 50 (2011) 1628.
39. J. Liu, Y. Wan, C. Liu, W. Liu, S. Ji, Y. Zhou and J. Wang, *European Journal of Inorganic Chemistry*, 2012 (2012) 3825.